Brief Review

Modern Physics Letters B, Vol. 24, No. 1 (2010) 1–28

World Scientific
www.worldscientific.com

USING NEUTRON DIFFRACTION AND MÖSSBAUER SPECTROSCOPY TO STUDY MAGNETIC ORDERING IN THE $R_3T_4Sn_4$ FAMILY OF COMPOUNDS

D. H. RYAN

Physics Department and Centre for the Physics of Materials, McGill University, 3600 University Street, Montreal, Quebec H3A 2T8, Canada

J. M. CADOGAN

Department of Physics and Astronomy, University of Manitoba, Winnipeg, Manitoba, R3T 2N2, Canada

C. J. VOYER

Physics Department and Centre for the Physics of Materials, McGill University, 3600 University Street, Montreal, Quebec H3A 2T8, Canada

M. NAPOLETANO

Dipartimento di Chimica e Chimica Industriale, Via Dodecaneso 31, 16146 Genova, Italy

P. RIANI

INSTM and Dipartimento di Chimica e Chimica Industriale, Via Dodecaneso 31, 16146 Genova, Italy

L. M. D. CRANSWICK

Canadian Neutron Beam Centre, NRCC, Chalk River Laboratories, Chalk River, Ontario K0J 1J0, Canada

Received 3 November 2009

We review the complementary roles that ^{119}Sn Mössbauer spectroscopy and neutron diffraction are playing in developing a complete description of magnetic ordering in the $R_3Cu_4Sn_4$ and $R_3Ag_4Sn_4$ intermetallic compound series. We show that the two techniques yield consistent pictures of the order, and in many cases *both* are essential to obtaining a complete description. The recent neutron diffraction work on $Sm_3Cu_4Sn_4$, $Sm_3Ag_4Sn_4$ and $Gd_3Ag_4Sn_4$ is highlighted.

Keywords: Mossbauer spectroscopy; neutron diffraction; rare-earths; intermetallic compounds; magnetic order.

1. Introduction

Mössbauer spectroscopy and neutron diffraction play complementary roles in the study of magnetic order in rare-earth intermetallics. The first provides local information on magnetic environments through both the hyperfine field (either intrinsic in the case of magnetic ions, such as many of the rare earths, or transferred in the case of non-magnetic probes, such as tin) and the electric field gradient. The second yields values for ordered moments and a description of the long-range magnetic order. Each technique has strengths and weaknesses, and while neutron diffraction remains the method of choice for investigating magnetic order in rare-earth intermetallics, its blanket sensitivity to all structural and magnetic changes occurring in the sample can make interpretation of the data quite challenging. This is especially true when two or more magnetic species are present, or when structure factor effects lead to weak or highly distributed magnetic scattering. By contrast, Mössbauer spectroscopy cannot be used directly to determine the nature of the long-ranged ordered state as it is *local* probe, but this limitation brings many advantages as it remains exquisitely sensitive to the *presence* of magnetic order and is unlikely to be blinded by long-range complexities. Both methods are quantitative and provide phase specific data, crucial when impurity effects may be present, and as we will show in the examples below, they are most effective when they are used together.

The orthorhombic $R_3T_4X_4$ family (where R is a rare earth, T = Cu, Ag, Au, and X = Si, Ge, Sn) represents an extensive series of isostructural compounds that exhibits a rich variety of magnetic ordering. They crystallize in an orthorhombic $Gd_3Cu_4Ge_4$-type structure (space group *Immm*, #71).[1] The rare earth atoms occupy two crystallographically distinct sites (4e and 2d), with the transition metal (T) on the 8n site and the X atoms filling two sites (4h and 4f). In general, the rare earth moments order antiferromagnetically (AF), often with quite different moment values,[2–6] and with distinct magnetic structures being adopted by the two rare earth sublattices. In some cases the two rare earth sites will also have quite different ordering temperatures.[7]

The complexity of the magnetic ordering exhibited by the $R_3T_4X_4$ series makes identifying the nature of the order quite challenging, however in some cases it is even difficult to locate the onset of magnetic order with any certainty as conventional bulk magnetic measurements, such as susceptibility or magnetization, can fail to yield an unambiguous signature. Two striking examples of this are provided by $Sm_3Ag_4Sn_4$ where the transition was revised[8] from $\sim$9 K to 26 K on the basis of ^{119}Sn Mössbauer data,[9] and $Gd_3Ag_4Sn_4$ where the transition was revised[8] from $\sim$8 K to $\sim$29 K on the basis of both ^{119}Sn Mössbauer data[10] and neutron diffraction work.[11] In both cases, there are clear magnetic events that reflect reorientations, but only extremely weak susceptibility markers of the onset of long-ranged order. Heat capacity has also been used to locate magnetic transitions in several compounds,[12,13] however, even here there are difficulties and, as we will show below, the situation in $Sm_3Cu_4Sn_4$ is quite different from that originally inferred from χ_{ac} or heat capacity data.[13]

In the examples that follow, we will show how data from ^{119}Sn Mössbauer spectroscopy have been used to develop a much clearer understanding of the magnetic ordering in the $R_3T_4Sn_4$ system. In doing this, in no way do we intend to argue that Mössbauer spectroscopy should replace neutron diffraction; indeed all of the systems presented here have been actively studied by neutron diffraction. We wish rather to demonstrate that neutron diffraction should not be used in isolation, and that by bringing more than one technique to bear on a problem, a much clearer and unambiguous picture emerges.

2. Experimental Methods

The silver-based compounds were prepared by induction melting stoichiometric quantities of the pure elements (rare earth 99.9 wt.%, Ag and Sn 99.999 wt.%) in sealed tantalum crucibles under high-purity argon. The alloyed buttons were then sealed under vacuum in quartz tubes, annealed for 20 days at 873 K and quenched in water. Cu-K_α X-ray diffraction and electron microprobe analysis confirmed the majority phase to be the intended orthorhombic $R_3X_4Sn_4$ compound. Refinement of the X-ray diffraction patterns showed the presence of less than 2 wt.% of the ζ-phase $Ag_{79}Sn_{21}$.

The copper-based compounds were prepared in a tri-arc furnace with a base pressure of better than 6×10^{-7} mbar. Stoichiometric amounts of pure elements (Cu 99.9 wt.%, others as above) were melted several times under pure (< 1 ppm impurity) argon to ensure homogeneity. The ingots were sealed in quartz tubes with a partial pressure of He, annealed at 1073 K for one week and water quenched. Small amounts (usually less than 2 wt.%) of a RCu_2Sn_2 impurity phase were detected by Cu-K_α X-ray diffraction.

Basic magnetic characterization was carried out on a Quantum Design PPMS system. ^{119}Sn transmission Mössbauer spectra were collected on a constant acceleration spectrometer using a 0.4 GBq ^{119m}Sn $CaSnO_3$ source with the samples either in a helium flow cryostat ($T < 20$ K) or a vibration-isolated closed-cycle refrigerator ($T > 20$ K). The spectrometer was calibrated using a ^{57}Co**Rh** source and an α-Fe foil. The spectra were fitted using a conventional nonlinear least-squares minimization routine with line positions and intensities calculated from a full Hamiltonian solution.[14]

Neutron diffraction measurements were made using the C2 multi-wire powder diffractometer on the NRU reactor at the Chalk River Laboratories, Ontario Canada. Temperatures down to 3.7 K were obtained using a closed-cycle refrigerator. Two neutron wavelengths ($\sim$1.33 Å and $\sim$2.37 Å) were used to cover a q-range of 0.2 Å^{-1} to 8 Å^{-1} in two 80° banks. The samples were mounted in conventional 5 mm inside diameter vanadium cans, except for the Sm and Gd based compounds where the extreme neutron absorption of these elements necessitated a different approach. For these materials we used a large-area flat-plate holder with single crystal silicon windows that was developed to work with highly absorbing samples.[15] This

Table 1. Lattice parameters for the orthorhombic $R_3Cu_4Sn_4$ compounds.

Compound	*a* (Å)	*b* (Å)	*c* (Å)	Ref.
$Ce_3Cu_4Sn_4$	14.903(3)	6.925(1)	4.542(1)	4
$Pr_3Cu_4Sn_4$	15.004(7)	6.981(3)	4.567(2)	20
$Nd_3Cu_4Sn_4$	14.964(5)	6.976(2)	4.545(1)	20
$Sm_3Cu_4Sn_4$	14.856	6.968	4.520	13
$Gd_3Cu_4Sn_4$	14.743(4)	6.939(2)	4.4736(11)	10
$Tb_3Cu_4Sn_4$	14.6655(9)	6.9183(4)	4.4470(3)	2
$Dy_3Cu_4Sn_4$	14.612(1)	6.9110(5)	4.4312(3)	2
$Ho_3Cu_4Sn_4$	14.5744(8)	6.9052(3)	4.4187(2)	2
$Er_3Cu_4Sn_4$	14.5327(8)	6.8978(3)	4.4050(2)	2

Note: the data for $Ce_3Cu_4Sn_4$ were taken at 12 K, the remainder are ambient temperature values.

Table 2. Lattice parameters for the orthorhombic $R_3Ag_4Sn_4$ compounds at ambient temperatures.

Compound	*a* (Å)	*b* (Å)	*c* (Å)	Ref.
$Ce_3Ag_4Sn_4$	15.547(8)	7.362(3)	4.679(1)	21
$Pr_3Ag_4Sn_4$	15.451(4)	7.349(2)	4.654(1)	5
$Nd_3Ag_4Sn_4$	15.404(6)	7.339(3)	4.632(2)	5
$Sm_3Ag_4Sn_4$	15.300(3)	7.324(2)	4.597(1)	9
$Gd_3Ag_4Sn_4$	15.223(4)	7.309(2)	4.565(1)	10
$Tb_3Ag_4Sn_4$	15.1581(4)	7.3034(17)	4.5502(11)	22
$Dy_3Ag_4Sn_4$	15.1150(32)	7.2826(13)	4.5296(8)	6

holder allowed us to place about 1.6 g (Sm-based compounds) and about 300 mg (Gd-based compounds) of sample in the 8 cm × 2.4 cm beam and obtain a usable scattering signal.

Refinement of the Cu K_α X-ray diffraction patterns and the non-magnetic neutron diffraction patterns was carried out using GSAS[16] via the EXPGUI[17] user interface to extract lattice parameters (Tables 1 and 2) and to check sample purity. All refinements of the magnetic neutron diffraction patterns were carried out using the FULLPROF/WinPlotr package[18,19] and analysis of the neutron diffraction patterns included a correction for the rather high neutron absorption by Dy. The patterns from the Gd and Sm-based compounds were truncated at 60°–2θ to minimize the effects of angle dependent absorption effects from the flat plate geometry on the observed peak intensities.

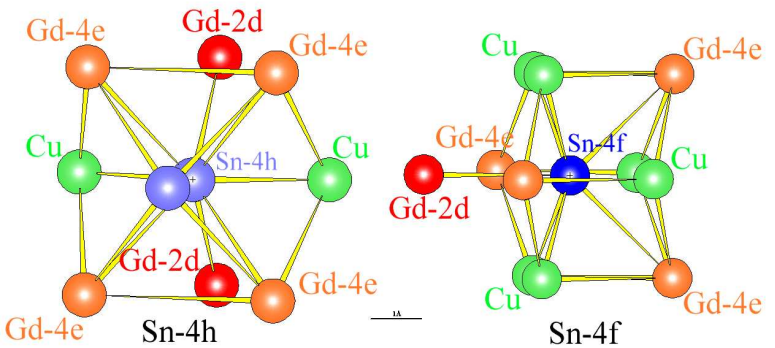

Fig. 1. Tin coordination shells for the Sn-4h (left) and Sn-4f (right) sites in $Gd_3Cu_4Sn_4$. Both tin sites have four Gd-4e neighbors, but the Sn-4f has only a single Gd-2d neighbor. The 1 Å bar (bottom center) provides a scale. The *c*-axis is approximately vertical.

3. General Considerations

Tin atoms carry no local moment of their own, so all observed magnetic splittings in $R_3T_4Sn_4$ are the result of hyperfine fields transferred from the moments on the neighboring rare earth sites. As the tin atoms occupy sites with identical crystallographic multiplicities, spectral area cannot be used to distinguish the two contributions to the spectra, however, the coordination of the two tin sites is sufficiently different that in many cases site assignments can be made. Figure 1 shows that the Sn-4h site has two rare-earth 2d neighbors (R-2d) and four equidistant R-4e neighbors, while the Sn-4f site has a single R-2d neighbor and four R-4e neighbors (in two sets of equidistant pairs, one approximately 0.5 Å further than the other depending on the lattice parameters). Given the frequency of independent ordering at the two R sites in these compounds, and the fact that it is the R-2d that generally orders at the higher temperature when separate ordering occurs, the single R-2d neighbor of the Sn-4f site is particularly valuable: *any* ordering of the R-2d moments *must* lead to a magnetic hyperfine field at the Sn-4f site. By contrast, the complex magnetic structures adopted by these compounds frequently leads to magnetic environments around the tin atoms in which the contributions from the R-4e moments cancel at one (e.g. $Nd_3Ag_4Sn_4$)[23] or even both (e.g. $Ho_3Cu_4Sn_4$)[23] of the tin sites.

One very simple way to estimate the magnitudes of the transferred hyperfine fields at the two tin sites, if the magnetic structure is known, is to assume that the transfer process is purely isotropic and to construct a vector sum of the first neighbor moments (ignoring the small variations in distance, but taking account of the different moment sizes). As can be seen in Table 3, this process leads to a quite reasonable agreement with the observed field ratios, and can therefore be used to assign the observed subspectra to specific tin sites. The special case of $Sm_3Ag_4Sn_4$,[9] where a significant contribution to B_{hf} must come from anisotropic transfer[24,25]

Table 3. Calculated isotropic transferred hyperfine field ratios compared with measured hyperfine fields (B_{hf}) at the two tin sites in $R_3T_4Sn_4$.

Compound	Sn-4h:Sn-4f (isotropic)	Ref.	Sn-4h:Sn-4f B_{hf} ratio	Ref.
$Pr_3Cu_4Sn_4$	1.17	20	—	
	3.1 (aniso)	20	4.56	26
$Nd_3Cu_4Sn_4$	—	—	1.74	23
$Nd_3Ag_4Sn_4$	5.55	5	4.11	23
$Sm_3Cu_4Sn_4$	complex			26
$Sm_3Ag_4Sn_4$	0	9	—	
	0.57 (aniso)	9	0.37	9
$Gd_3Cu_4Sn_4$	complex			10
$Gd_3Ag_4Sn_4$	2	11	2.08	10
$Tb_3Cu_4Sn_4$	—	2	—	26
$Tb_3Ag_4Sn_4$	complex	22	2.07	22
$Dy_3Cu_4Sn_4$	—	2	—	9
$Dy_3Ag_4Sn_4$	Sn-4h$_1$:Sn-4h$_2$:Sn-4f 1.98:0.58:1	6	Sn-4h$_1$:Sn-4h$_2$:Sn-4f 3.42:2.0:1	6
$Ho_3Cu_4Sn_4$	2	27	2.17	23
$Er_3Cu_4Sn_4$	2	2	2.86	7

Note: $Sm_3Cu_4Sn_4$ exhibits slow paramagnetic relaxation effects and does not form a long-ranged ordered state above 3.6 K,[26] while $Tb_3Ag_4Sn_4$ undergoes a first-order orthorhombic → monoclinic distortion on cooling.[22] The cell-doubled magnetic order in $Dy_3Ag_4Sn_4$ leads to a subsplitting of the Sn-4h crystallographic site into two magnetically distinct sub-sites (Sn-4h$_1$ and Sn-4h$_2$). The anisotropic contribution to the transferred hyperfine field appears to dominate for $Pr_3Cu_4Sn_4$ and $Sm_3Ag_4Sn_4$, so both isotropic and anisotropic field ratios are given in these cases.

will be discussed below. Where the magnetic structure is not known, the hyperfine field ratio can be used to restrict the set of possible structures.

^{119}Sn Mössbauer spectroscopy is particularly sensitive to the onset of magnetic order, especially at the R-2d site, and in some cases it is more sensitive than neutrons. We will describe two very different example $Nd_3Cu_4Sn_4$ (Ref. 23) and $Sm_3Ag_4Sn_4$,[9] where neutron diffraction has encountered difficulties. However there is one other situation in which ^{119}Sn Mössbauer spectroscopy provides unique insights: when long-ranged order does not develop at all. $Sm_3Cu_4Sn_4$ (Ref. 26) shows only slow paramagnetic relaxation effects and does not order above 3.6 K, thus neutron diffraction, which relies on the presence of long-ranged periodic magnetic order, yields no magnetic signal despite clear indications of magnetic effects in both susceptibility and heat capacity.[13]

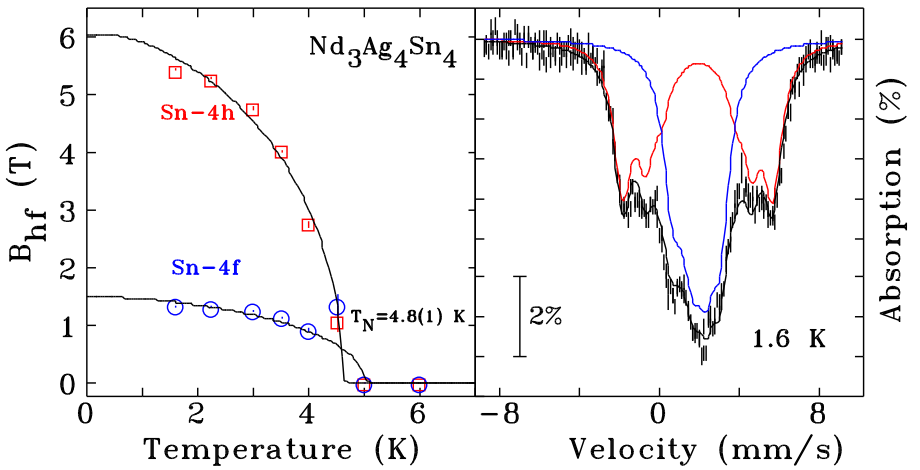

Fig. 2. Left: Temperature dependence of the hyperfine fields at the two tin sites in $Nd_3Ag_4Sn_4$ showing an average transition temperature of 4.8(1) K. The solid lines are fits to $J = \frac{9}{2}$ Brillouin functions. Right: ^{119}Sn Mössbauer spectrum at 1.6 K with the components assigned to the Sn-4h and Sn-4f site shown separately.

4. Some Simple Examples

4.1. *$Nd_3Ag_4Sn_4$*

Both Nd sites in $Nd_3Ag_4Sn_4$ order together at 5 K, adopting independent antiferromagnetic structures with quite different moments.[5] The 1.3 μ_B Nd-2d moments order parallel to the a-axis, while the 2.3 μ_B Nd-4e moments lie in the ab plane making an angle of 144° with the a-axis. The ^{119}Sn Mössbauer spectrum at 1.6 K (right panel of Fig. 2) shows two equal area components with fields of 5.43(2) T and 1.32(2) T consistent with the crystallographic populations of the two tin sites. Tracking the temperature dependence of the two hyperfine fields (left panel of Fig. 2) yields an average ordering temperature of 4.8(1) K consistent with the neutron diffraction results. We can use the known magnetic structure[5] to estimate the transferred fields at the two tin sites. The Sn-4h site has two Nd-2d (1.3 μ_B) neighbors oriented parallel to the a-axis and four Nd-4e (2.3 μ_B) neighbors aligned in the ab plane, making an angle of 144° with the a-axis. However, the four Nd-4e neighbors of the Sn-4f site occur as two anti-parallel pairs and their contribution should cancel, leaving only a single Nd-2d moment to affect the Sn-4f site. If we assume, as discussed above, that the local field is simply a vector sum over the magnetic neighbors (including the different magnitudes of Nd moments) then we estimate a Sn-4h:Sn-4f field ratio of 5.6:1 which compares well with the observed ratio of 4.11(6):1 and allows us to assign the higher field component to tin atoms in the Sn-4h site.

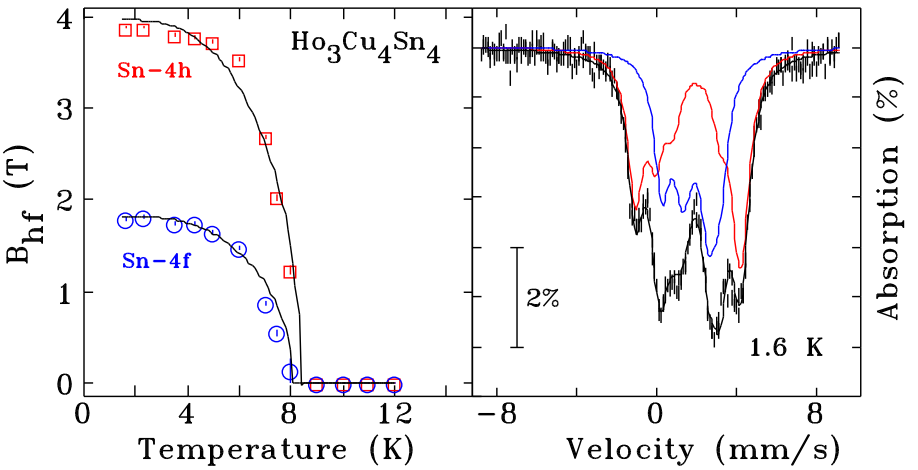

Fig. 3. Left: Temperature dependence of the hyperfine fields at the two tin sites in $Ho_3Cu_4Sn_4$ showing an average transition temperature of just over 8 K. The solid lines are fits to $J = \frac{1}{2}$ Brillouin functions (see text). Right: ^{119}Sn Mössbauer spectrum at 1.6 K with the components assigned to the Sn-4h and Sn-4f site shown separately.

4.2. *$Ho_3Cu_4Sn_4$*

$Ho_3Cu_4Sn_4$ exhibits more complex ordering[27] with the Ho-2d and Ho-4e sublattices reported to order at separate temperatures (7.6 K and 3.3 K respectively) and each undergoing at least one reorientation below their initial ordering events. Examination of the 1.6 K ^{119}Sn Mössbauer spectrum (right panel of Fig. 3) reveals an immediate difference from $Nd_3Ag_4Sn_4$: not only does the larger-field site have a smaller splitting, but the ratio of the two fields is clearly smaller (Table 3). We find that $J = \frac{1}{2}$ Brillouin functions (rather than the expected $J = 8$) give the best fits to the basic trends up to ∼8 K (left panel of Fig. 3) and yield an average ordering temperature of 8.2(1) K, consistent with magnetization data, but somewhat above that inferred from heat capacity. There is a weak break from the smooth curves near 6 K that might be associated with a reorientation of the Ho-2d sublattice, but the effect is small.

Examination of the complex magnetic structure adopted by the Ho-4e moments leads us to expect that their contribution to the transferred hyperfine field at *both* tin sites will be zero. The two Ho-2d neighbors of the Sn-4h site are parallel to each other, and the Sn-4f site has a single Ho-2d neighbor, leading to a simple prediction of a 2:1 field ratio for Sn-4h:Sn-4f. The observed ratio at 1.6 K is 2.17(3):1, and this allows us to assign the higher field component to the Sn-4h site.

4.3. *$Nd_3Cu_4Sn_4$*

$Nd_3Cu_4Sn_4$ provides a third relatively simple example of magnetic ordering in the $R_3T_4Sn_4$ compound series. It also serves to illustrate the power of ^{119}Sn Mössbauer

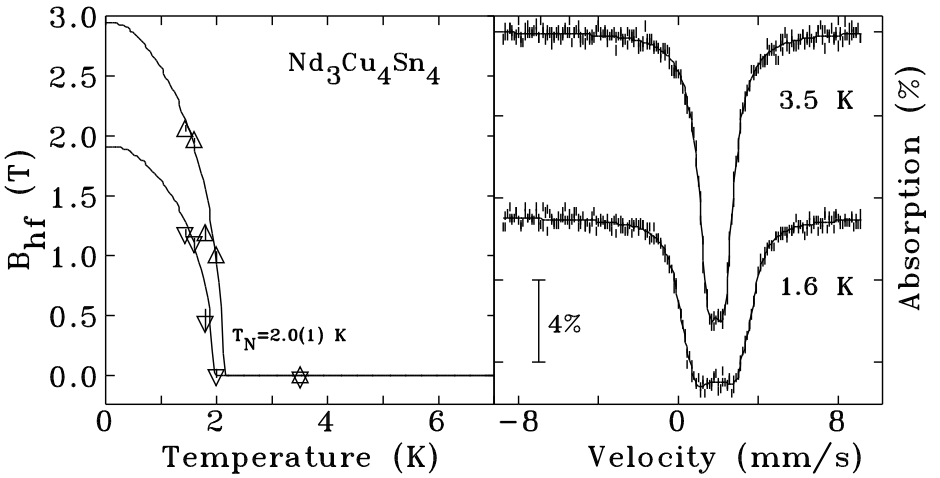

Fig. 4. Left: Temperature dependence of the hyperfine fields at the two tin sites in $Nd_3Cu_4Sn_4$ showing an average transition temperature of 2.0(1) K. The solid lines are fits to $J = \frac{9}{2}$ Brillouin functions (see text). Right: ^{119}Sn Mössbauer spectra at 1.6 K and 3.5 K showing the clear changes in both the overall form and the maximum absorption as magnetic order appears.

spectroscopy in detecting magnetic order. Heat capacity and susceptibility measurements both place the onset of magnetic order at 1.8 K,[13] however a more recent neutron diffraction study failed to find any magnetic scattering at 1.5 K.[20] It is immediately clear from the 1.6 K spectrum shown in Fig. 4 that a magnetic splitting is present at that temperature. Moreover, tracking the temperature dependence of the observed splitting yields an estimated ordering temperature of 2.0(1) K, fully consistent with the previously reported values. The observed hyperfine fields are not especially small and more than 50% of the extrapolated maximum has been achieved by 1.45 K (our lowest temperature), so it is unclear why no magnetic signal was observed in the neutron diffraction pattern. It is possible that $Nd_3Cu_4Sn_4$ adopts a complex magnetic structure that leads to distributed and therefore fairly weak scattering, but resolution of this discrepancy awaits a more detailed neutron diffraction study. An initial measurement at 0.38 K did show clear magnetic contributions[28] so the material does indeed order magnetically. Finally, we note that the observed field ratio of 1.74:1 suggests that we are seeing only the effects of the Nd-2d moments and that the Nd-4e sublattice is either not ordered or it adopts a magnetic structure that leads to a cancellation at the two tin sites (as is the case in $Ho_3Cu_4Sn_4$).

5. More Complex Examples

The compounds discussed in the previous section all exhibit relatively simple ordering effects, at least as far as the ^{119}Sn Mössbauer spectra are concerned, and the Mössbauer work was done after an initial or complete neutron diffraction study had been carried out. The next two examples were studied in parallel, using results from

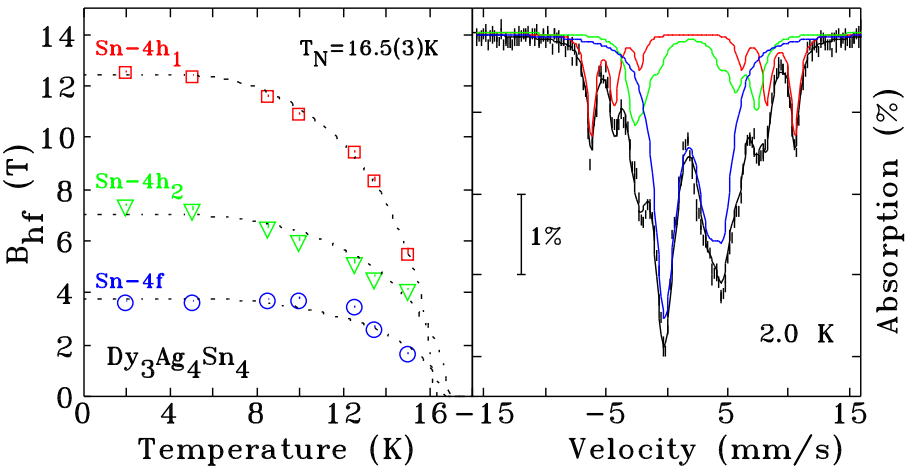

Fig. 5. Left: Temperature dependence of the hyperfine fields for the three components observed in the ^{119}Sn Mössbauer spectra of $Dy_3Ag_4Sn_4$. The two larger field components (□ and ▽) each account for 25% of the total area, while the third component (◯) accounts for the rest. The solid lines are fits to Brillouin functions that yield an average ordering temperature of 16.5(3) K. Site assignments are discussed in the text. Right: ^{119}Sn Mössbauer spectrum of $Dy_3Ag_4Sn_4$ at 2.0 K. The outer component (lines at ±6 mm/s) is clearly weaker than would be expected for a subspectrum contributing 50% of the total area — compare this with the 1.6 K spectra of $Nd_3Ag_4Sn_4$ (Fig. 2) or $Ho_3Cu_4Sn_4$ (Fig. 3). The components assigned to the Sn-4h$_1$, Sn-4h$_2$ and Sn-4f are shown separately.

neutron diffraction and ^{119}Sn Mössbauer spectroscopy each to aid in understanding the other.

5.1. *$Dy_3Ag_4Sn_4$*

χ_{ac} places the onset of ordering in $Dy_3Ag_4Sn_4$ at ∼15 K, with no evidence of further changes at least down to 1.7 K.[6] The 2 K ^{119}Sn Mössbauer spectrum (Fig. 5) is clearly magnetically split, but it cannot be fitted with a simple pair of equal-area sextets. This is easily seen by examining the outer sextet: the lines are simply too weak to account for half of the total area. We found that a three site model with an area ratio of 1:1:2 (in order of decreasing field magnitude) gave an excellent fit, and tracking the fitted hyperfine fields as a function of temperature (Fig. 5) gives an average transition temperature of 16.5(3) K, in good agreement with the χ_{ac} value. The sub-splitting into three components suggests that the magnetic structure of $Dy_3Ag_4Sn_4$ is more complex than it is in the previous examples and that it leads to one of the two *crystallographically* inequivalent sites dividing further into a pair of *magnetically* inequivalent sites.

Our neutron diffraction study[6] yields an ordering temperature of 16.5(5) K, fully consistent with that deduced from the ^{119}Sn Mössbauer data, but it also revealed more details. The diffraction patterns shown in Fig. 6 show the development of many strong magnetic reflections on cooling, but there are a number of peaks that

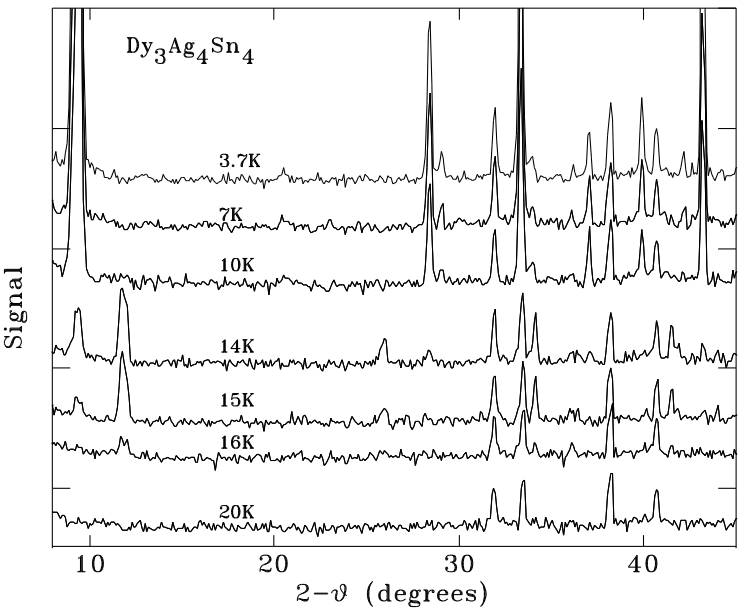

Fig. 6. Neutron diffraction patterns for $Dy_3Ag_4Sn_4$ at several temperatures taken with a wavelength of 2.3719Å. Several strong magnetic reflections appear on cooling below 20 K, and one, due to incommensurate order appears first, but is lost on further cooling.

appear first at incommensurate positions and subsequently vanish on further cooling. The temperature dependence of several commensurate and incommensurate peaks is shown in Fig. 7. It is clear that the initial order established in $Dy_3Ag_4Sn_4$ is incommensurate and only later does it adopt a commensurate structure. A fit to the temperature dependence of the commensurate peak intensities in Fig. 7 yields a transition temperature of 14.5(2) K.

Analysis of the diffraction pattern at 3.7 K shows that the magnetic structure is doubled along the *b*-axis. The 8.3(3) μ_B Dy-2d moments are aligned with the *a*-axis, while the 7.7(5) μ_B Dy-4e moments adopt a more complex structure lying in the *ab* plane.[6] On warming, the Dy-2d sublattice does not change structure, while it is the Dy-4e sublattice that becomes incommensurate.

It is not certain why the ^{119}Sn Mössbauer hyperfine fields in Fig. 5 do not reflect the 14.5 K transition seen by neutron diffraction, however it is likely that the line overlap caused by having three components with relatively modest splittings masks the effects so close to the initial onset of order at 16.5 K. Analysis of the magnetic structure deduced from the neutron diffraction pattern at 3.7 K reveals that all of the Sn-4f sites have the same magnetic environments, while the Sn-4h sites split into two equal sub-groups. This provides both an explanation for the observed subsplitting of the Mössbauer spectra and an independent confirmation of the deduced magnetic structure for $Dy_3Ag_4Sn_4$. The assignment of the sub-split components to the Sn-4h crystallographic site is also consistent with the tin atoms

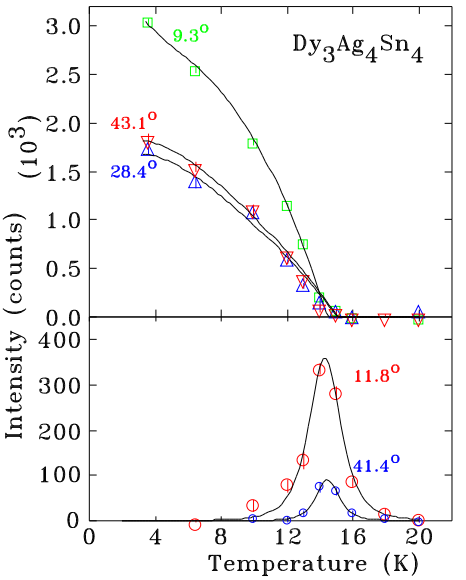

Fig. 7. Temperature dependence of several strong magnetic reflections for $Dy_3Ag_4Sn_4$. The upper panel shows the peaks associated with the low temperature commensurate ordering, while the lower panel shows those peaks associated with the incommensurate order that is present for $12\,K < T < 17\,K$.

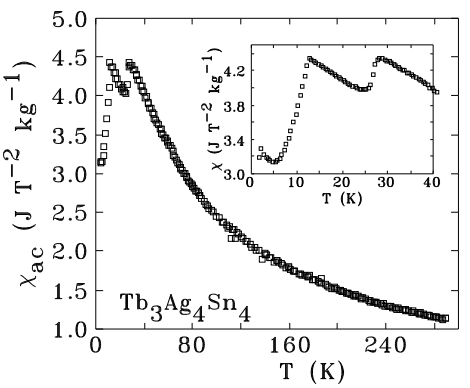

Fig. 8. AC susceptibility (χ_{ac}) as a function of temperature for $Tb_3Ag_4Sn_4$. The inset shows the region below 40 K in more detail. Two magnetic transitions at 13 K and 28 K are apparent.

in this site having the larger hyperfine field in almost all compounds where such an assignment can be made.

5.2. *$Tb_3Ag_4Sn_4$*

The behavior of $Tb_3Ag_4Sn_4$ is, so far, unique within the entire $R_3T_4X_4$ compound series. χ_{ac} shows two magnetic transitions (Fig. 8), at 13 K and 28 K, a relatively

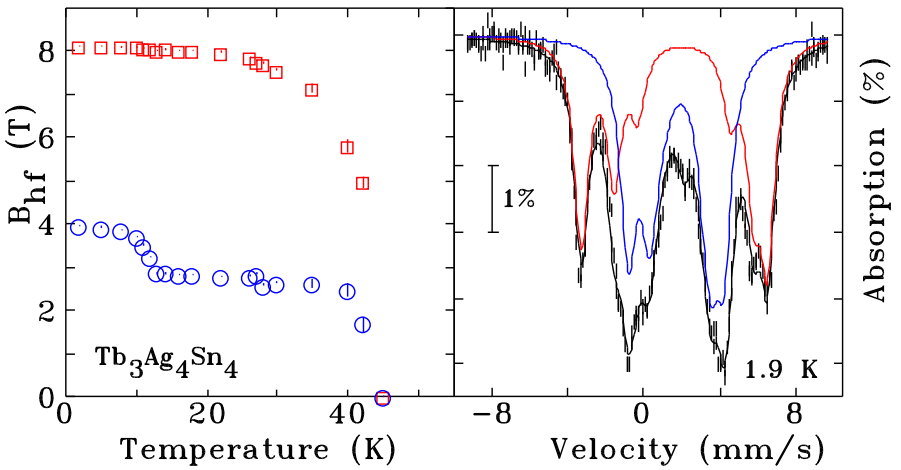

Fig. 9. Left: Temperature dependence of the hyperfine field (B_{hf}) at the two tin sites in $Tb_3Ag_4Sn_4$ showing the clear break at about 13.5 K for the lower field site, but no feature at the upper transition (28 K) seen in χ_{ac}(T). (Figure 8. Note the persistence of the magnetic splitting to over 40 K). Right: ^{119}Sn Mössbauer spectrum of $Tb_3Ag_4Sn_4$ at 1.9 K. The two equal-area components used to fit the pattern are also shown.

common feature of this series. Similarly, the ^{119}Sn Mössbauer spectrum at 1.9 K (Fig. 9) is unremarkable, showing two well-resolved, equal area sextets with a field ratio of 2.07:1, suggesting a structure in which the effects of the Tb-4e moments cancel at both tin sites, and the transferred hyperfine field is derived primarily from the Tb-2d moments. It is the temperature dependence of the two hyperfine fields in Fig. 9 that provides the first surprise: while there is a clearly resolved feature at the 13 K transition, *nothing* happens at 28 K where the initial ordering was expected to occur. Indeed the fields at both sites persist until ∼45 K, where χ_{ac}(T) is essentially featureless. As we will show in the final group of examples below, this inability of susceptibility to identify correctly the magnetic transitions in these compounds is remarkably common.

Figure 10 shows spectra at several temperatures for $Tb_3Ag_4Sn_4$ which reveal more details about the nature of the magnetic order in this compound. If one follows the leftmost peak in the pattern (at about −4 mm/s) one sees that as the temperature is increased, the peak does not move to the center as it would for a decreasing hyperfine field, but rather decreases in intensity. Indeed, by 35 K it has nearly vanished entirely, but its location has barely changed. The total fitted area of the two magnetic sites is plotted on the left panel of Fig. 10, where it is clear that the 28 K peak in the χ_{ac} data in Fig. 8 reflects the abrupt loss of the magnetic components. This behavior is more reminiscent of a first order magnetostructural transition than a conventional second order Néel transition. Neutron diffraction confirms this expectation.

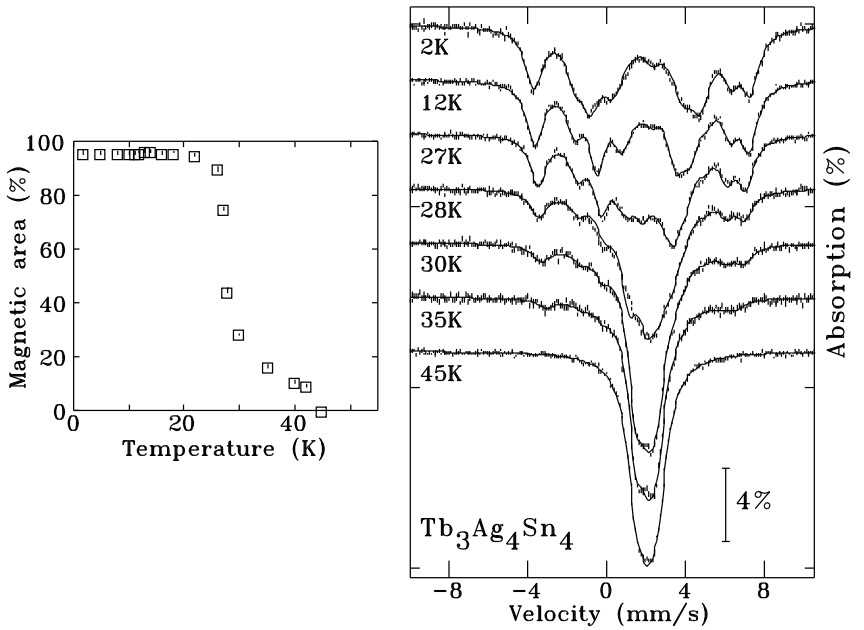

Fig. 10. Left: Temperature dependence of the magnetic area in the ^{119}Sn Mössbauer spectra of $Tb_3Ag_4Sn_4$. Note the clear break at about 28 K marking the first-order structural transition. Right: ^{119}Sn Mössbauer spectra of $Tb_3Ag_4Sn_4$ at several temperatures.

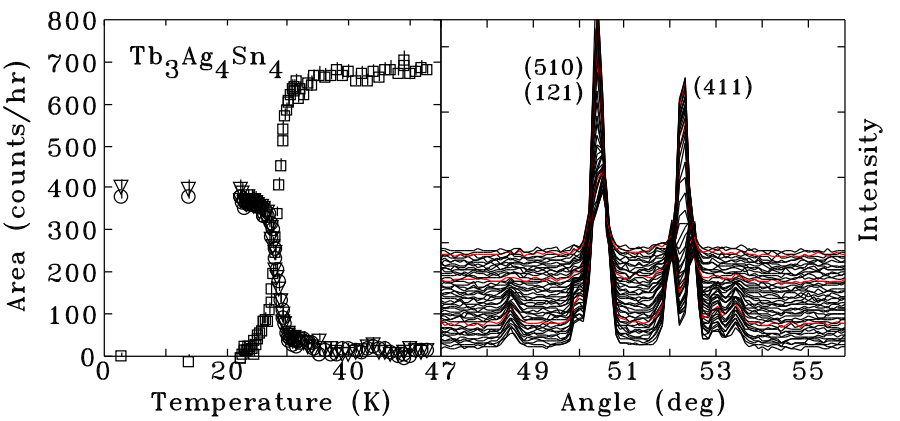

Fig. 11. (Color online) Left: Temperature dependence of the peaks near $2\theta = 52°$ showing the structural distortion that occurs at 28 K. Right: Series of neutron diffraction patterns for $Tb_3Ag_4Sn_4$ taken at a wavelength of 2.3724 Å. As the sample cools from 37 K (rear) to 22 K (front) the (411) peak near $2\theta = 52°$ splits as the sample undergoes a structural transformation from orthorhombic to monoclinic. The patterns at 35 K, 30 K and 25 K are plotted in red.

Figure 11 shows a small segment of the neutron diffraction pattern for $Tb_3Ag_4Sn_4$ on cooling from 37 K to 22 K. Some weak magnetic peaks develop at about 48.5° and just above 53°, while the overlapping (121) and (510)

reflections are unchanged. However it is the splitting of the (411) peak at 52.3° that is inconsistent with simple magnetic ordering. Examination of the full patterns reveals a very large number of changes on cooling through 28 K, as several peaks split and many new peaks appear. Unfortunately, the richness of the changes observed is actually too much information, as neutron diffraction is sensitive to both the structural *and* magnetic changes that are occurring, and with both happening simultaneously, it is not immediately obvious which are due to structure changes, and which reflect the magnetic ordering.

The solution was to turn to X-ray diffraction which is blind to the magnetic order and sees only the atomic structure. By combining the two diffraction techniques it has been possible to separate the magnetic and structural changes and determine that on cooling through 28 K, $Tb_3Ag_4Sn_4$ undergoes a structural transition from its room temperature orthorhombic $Immm$ form to a monoclinic C-centered structure (either Cc or $C2/c$). This transformation is accompanied by the development of magnetic order, suggesting that the ordering temperature of the monoclinic form is much higher than that of the parent orthorhombic structure. Indeed, enough of the monoclinic form persists on heating that we can estimate its ordering temperature using the data in Fig. 10 where the field goes to zero at about 45 K. We have no way of determining the ordering temperature of the parent orthorhombic form as it appears to be converted to the monoclinic form before it orders.

A detailed structural and magnetic refinement of this complex material is currently underway.

6. Special Cases: Where Neutrons Have Problems

Many of the rare earths have rather large absorption cross-sections for thermal neutrons and require special consideration when being used in a diffraction experiment. For example, dysprosium-based compounds ($\sigma_{abs} = 994$ barn[29]) are often run in narrower cans to reduce absorption losses, and it is essential that proper absorption corrections are applied during the analysis. However, Eu ($\sigma_{abs} = 4530$ barn[29]) and Sm ($\sigma_{abs} = 5922$ barn[29]) combine extreme absorption with small moments, making them both unattractive to use and very difficult to analyze. They are typically avoided. Finally, Gd ($\sigma_{abs} = 49700$ barn[29]) has nearly twenty times the absorption of cadmium. The metal has an absorption ($1/e$) length of about 7 μm and is far better suited to neutron shielding than scattering measurements. Attempts to make neutron diffraction measurements with Gd-based materials usually involve massive dilution (with Al or Si powders) to spread out a small sample, isotopic substitution (the even isotopes of Gd, while expensive, are much less absorbing) or short wavelength spectrometers (the absorption at 0.5 Å is much reduced, but the resolution is poor and most, if not all, of the low-q magnetic peaks are too close to the straight through beam to be observed). All of these approaches provide significant experimental challenges and yield weak scattering from small samples, or poorly resolved patterns from the short wavelengths used. As a result, few Gd-based compounds have been studied by neutron diffraction.

The absence of neutron diffraction data, combined with the problems encountered using bulk magnetic measurements to determine ordering temperatures, has left ^{119}Sn Mössbauer spectroscopy as the primary characterization tool available in these highly absorbing compounds. However, we recently developed a large-area flat-plate sample holder based on single-crystal Si plates that can be used for even Gd-based materials[30] and we will show examples of data obtained using this method for both Sm and Gd-based compounds.

6.1. $Sm_3Ag_4Sn_4$

Initial magnetization work on $Sm_3Ag_4Sn_4$ placed the onset of order at 9.1 K,[8] however there was a weak feature around 25 K that was not considered significant. Our more recent study[9] confirmed both features and found that a 24 K event was clearly present in the out of phase AC susceptibility (χ''), suggesting that it might be significant. As we will show here, the ordering temperature is 26 K, so in hindsight, the bulk measurements can be interpeted as "detecting" the transition. This failure of bulk magnetization measurements to yield an unambiguous signature even of the primary ordering was noted earlier in our discussion of $Tb_3Ag_4Sn_4$, and will recur in each of the three examples covered in this section.

The ^{119}Sn Mössbauer spectrum of $Sm_3Ag_4Sn_4$ at 2.2 K (Fig. 12) shows the expected two equal-area components, and the temperature dependence of the two hyperfine fields clearly confirms the two magnetic events detected by susceptibility. More significantly, the ^{119}Sn Mössbauer data demonstrate that the onset of order occurs at 26.0(5) K, and that the lower event at 8.3(3) K is due to a spin-

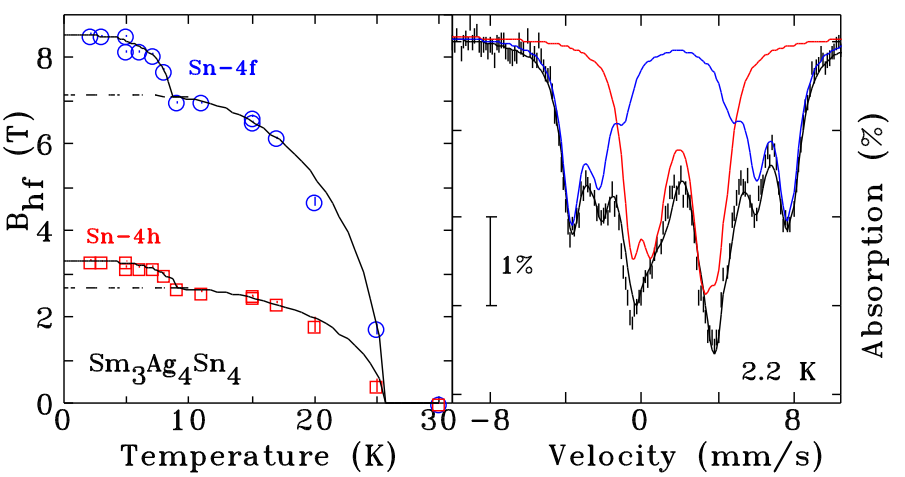

Fig. 12. Left: Temperature dependence of the hyperfine field (B_{hf}) at the two tin sites in $Sm_3Ag_4Sn_4$ showing the onset of order at 26.0(5) K and the clear break at 8.3(3) K that corresponds to the spin reorientation. Note the reversal of the site assignments as the Sn-4f is now the high-field component. Right: ^{119}Sn Mössbauer spectrum of $Sm_3Ag_4Sn_4$ at 2.2 K. The two equal-area components used to fit the pattern are also shown.

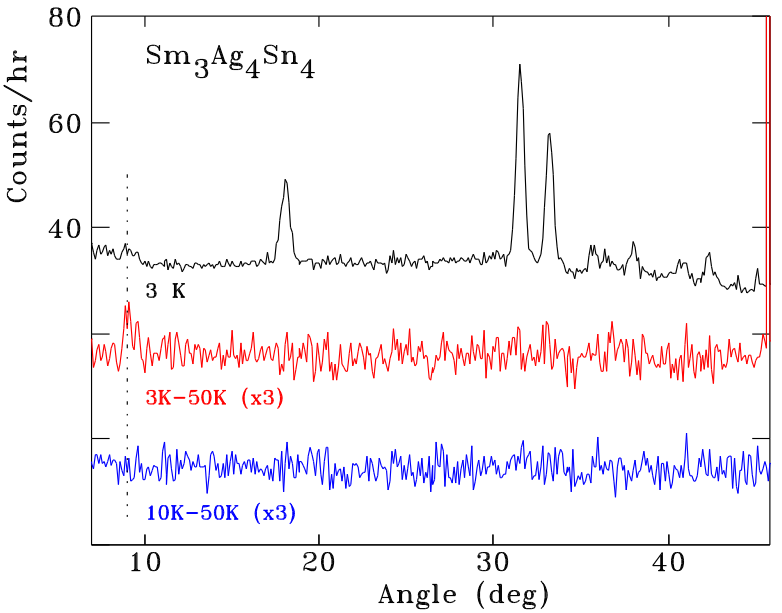

Fig. 13. Top: Neutron diffraction pattern for $Sm_3Ag_4Sn_4$ taken at 3 K showing a weak magnetic peak at $2\theta = 9°$ (dotted line). Middle: Difference between the 3 K and 50 K patterns (scaled by a factor of 3) to emphasize the magnetic peak. Bottom: Difference between the 10 K and 50 K patterns enlarged by the same factor of 3, showing no apparent magnetic signal. All measurements were made at a wavelength of 2.3722 Å.

reorientation, as there are breaks in both B_{hf}(T) and the fitted angle (θ) between the hyperfine field and the principal axis of the local electric field gradient (V_{zz})[9] at each site.

As noted above, neutron diffraction measurements on highly absorbing Sm-based compounds present special challenges, and the small moments typically encountered in samarium compounds led us to expect rather weak magnetic scattering. The flat-plate holder allowed us to place a total of 1.6 g of $Sm_3Ag_4Sn_4$ in the beam and obtain useful diffraction patterns at a wavelength of 2.3722 Å.[9] Figure 13 shows the diffraction pattern obtained at 3 K along with the differences between the 3 K and (non-magnetic) 50 K pattern which clearly shows that a single magnetic peak is observed at $2\theta = 9°$. This peak could be indexed as (100) and its temperature dependence gave a transition temperature of 8.3(4) K, consistent with the reorientation observed by ^{119}Sn Mössbauer spectroscopy at 8.3(3) K. No magnetic scattering is observed at 10 K (Fig. 13, lowest curve), however an analysis of the allowed commensurate orderings for this compound revealed that only two spin arrangements lead to a strong magnetic reflection, and that all others are characterized by a larger number of much weaker reflections. As we know that the sample is ordered up to 26 K, we conclude that the ordering belongs to one of these weak reflection modes for $9\,\mathrm{K} < \mathrm{T} < 26$ K.

Analysis of the magnetic environments of the two tin sites in $Sm_3Ag_4Sn_4$ for the two candidate magnetic structures shows that the isotropic contribution at the Sn-4h site is zero in both cases, and that the anisotropic contribution[24,25] is only non-zero for one of the possible structures (I_pmmm'), permitting an unambiguous determination of the magnetic structure by combining ^{119}Sn Mössbauer spectroscopy with neutron diffraction. While the Sn-4h sites only experience an anisotropic transferred field, the Sn-4f sites have a larger anisotropic contribution and an additional parallel isotropic contribution, leading us to assign the higher field site in Fig. 12 to the Sn-4f site. This is the reverse of the situation in all other compounds studied to date.

The I_pmmm' structure only permits ordering of the Sm-4e sites (a very rare situation in the $R_3T_4X_4$ system, where it is normally the R-2d site that orders first), and places the moments parallel to the *b*-axis. The loss of the (100) peak on heating through 8 K reflects a rotation of the ordering direction towards the *a*-axis, and not a loss of magnetic order, as the ^{119}Sn Mössbauer spectra clearly show a significant magnetic splitting up to 26 K. With the structure identified, it was also possible to estimate the Sm moment and we obtained a Sm-4e moment of $0.47\pm0.10\,\mu_B$ at 3 K.[9]

6.2. $Sm_3Cu_4Sn_4$

The magnetic behavior of $Sm_3Cu_4Sn_4$ is surprisingly different from that of $Sm_3Ag_4Sn_4$ described above, and serves to provide an example of a limitation inherent to neutron diffraction beyond the obvious, and quite severe problems caused by the highly absorbing samarium. Susceptibility and heat capacity appear to indicate the presence of several magnetic transitions, starting at 9 K followed by another at 7.5 K and finally a first-order event at 5 K.[13] The ^{119}Sn Mössbauer spectrum at 1.6 K presents the usual two equal-area magnetic sub-spectra with quite substantial fields (Fig. 14). The temperature dependence of the hyperfine fields shows no apparent evidence of the three events previously identified at 9 K and below, and a magnetic splitting persists in the spectra until at least 40 K, well beyond any expected ordering temperature.

The neutron diffraction pattern, measured using the same flat-plate sample holder as before, shows no evidence of magnetic order (Fig. 15). Indeed, the difference between the 3 K and 20 K patterns is flat apart from statistical fluctuations, and appears more consistent with a paramagnetic state at 3 K.

A visual inspection of the ^{119}Sn Mössbauer spectra shown in Fig. 16 reveals some unusual changes on heating: rather than simply moving together as the hyperfine field decreases with increasing temperature, the outer lines seem to broaden and become less distinct, while the central region fills in. Attempting to model this behavior using a pair of gaussian distributions of hyperfine fields yields adequate fits but the derived parameters do not follow expected trends.

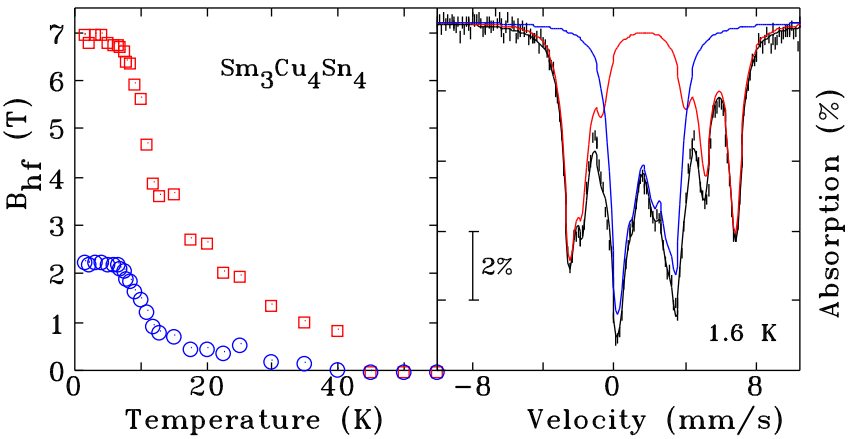

Fig. 14. Left: Temperature dependence of the hyperfine field (B_{hf}) at the two tin sites in $Sm_3Cu_4Sn_4$ showing a weak break around 10 K, but with significant fields persisting to at least 40 K. Right: ^{119}Sn Mössbauer spectrum of $Sm_3Cu_4Sn_4$ at 1.6 K. The two equal-area components used to fit the pattern are also shown.

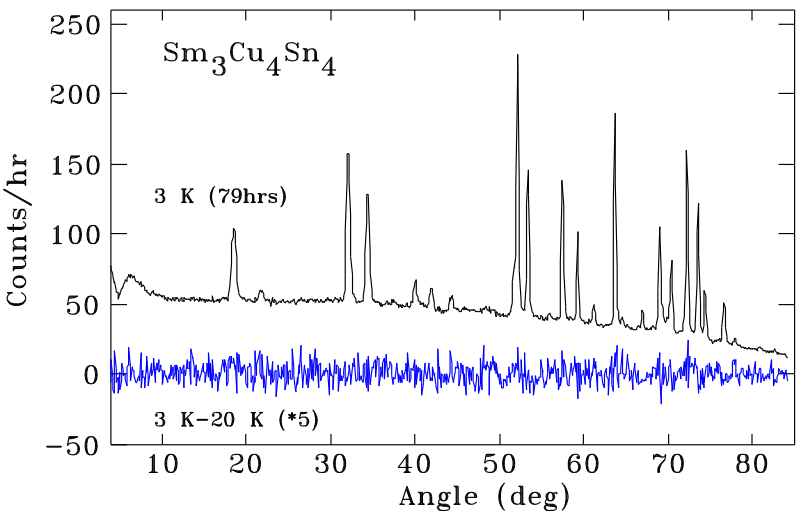

Fig. 15. Top: Neutron diffraction pattern for $Sm_3Cu_4Sn_4$ taken at 3 K showing clearly resolved nuclear peaks, but no apparent magnetic scattering. Bottom: Difference between the 3 K and 20 K patterns (scaled by a factor of 5) to emphasize the absence of magnetic scattering. Measurements were made at a wavelength of 2.3715 Å.

The fitted widths of the two distributions (left panel of Fig. 17) increase abruptly at about 5 K, and then decrease gradually above about 10 K. However it is the behavior of the subspectral area, shown in the right panel of Fig. 17, that is unphysical. In all of the $R_3T_4Sn_4$ compounds discussed here, it is possible to fit the spectra using two (or in one case, $Dy_3Ag_4Sn_4$, three) subspectra with well defined areas that

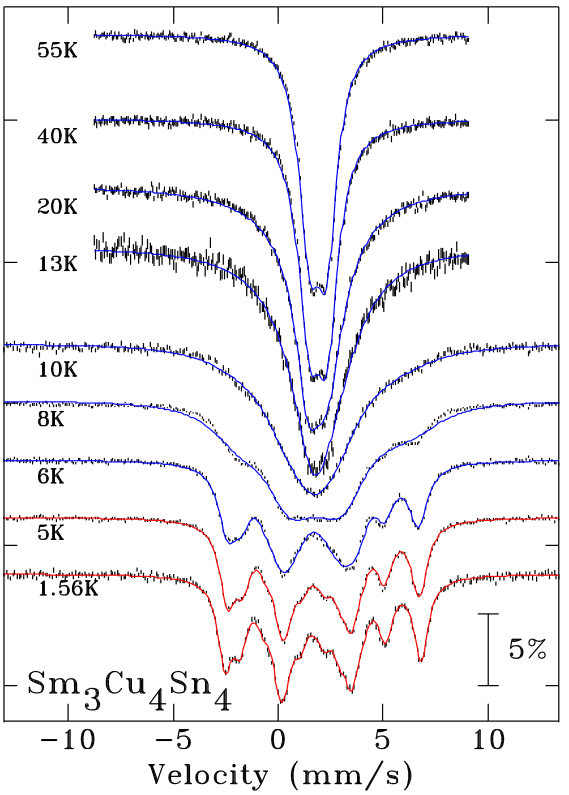

Fig. 16. (Color online) ^{119}Sn Mössbauer spectra of $Sm_3Cu_4Sn_4$ for various temperatures. Solid lines are the result of dynamic fits (blue) for $T \geq 6$ K, and static fits (red) for $T \leq 5$ K (see text).

remain relatively stable as a function of temperature, even if they are left as free parameters in the fit. This process fails here, and we see the low-field component becoming completely dominant as the distributions broaden. This behavior, taken with the appearance of the spectra, leads to another possible approach — dynamic relaxation.

Fitting the spectra using a conventional dynamic up/down relaxation model[31] yields good results for $T \geq 6$ K, however below this, the fitted fluctuation rates are so slow as to be effectively static and a static model was used for the lowest temperatures. The fits shown through the spectra in Fig. 16 reflect this distinction. We emphasize that the change in model used at low temperatures is solely for operational convenience and is based on the observation that the fluctuation rates are too slow to be resolved. It *does not* mean that we believe that the samarium moments are actually static, or that they have formed a long-range ordered state. Indeed, the trend in relaxation rates shown in Fig. 18 shows a fairly steady decline on cooling and it is likely that this trend continues once it passes below our ability to resolve it.

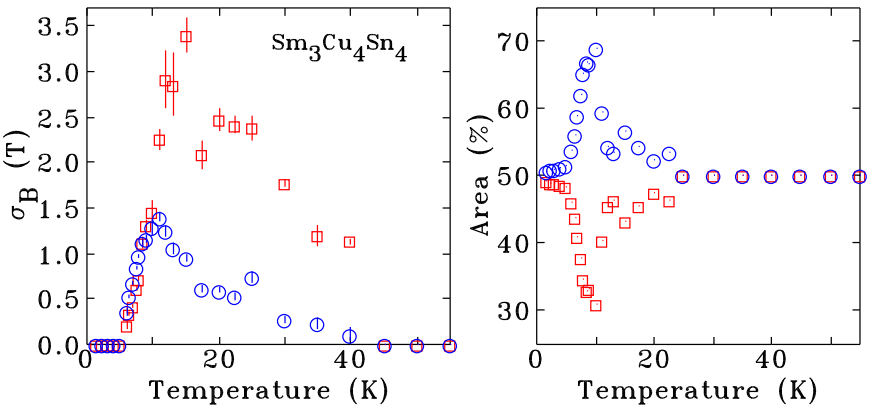

Fig. 17. Left: Temperature dependence of the width of the two gaussian hyperfine field distributions (σ_B) used to fit the ^{119}Sn Mössbauer spectra of $Sm_3Cu_4Sn_4$. Right: Areas of the two components used showing the clear departure from the expected 50%:50% ratio.

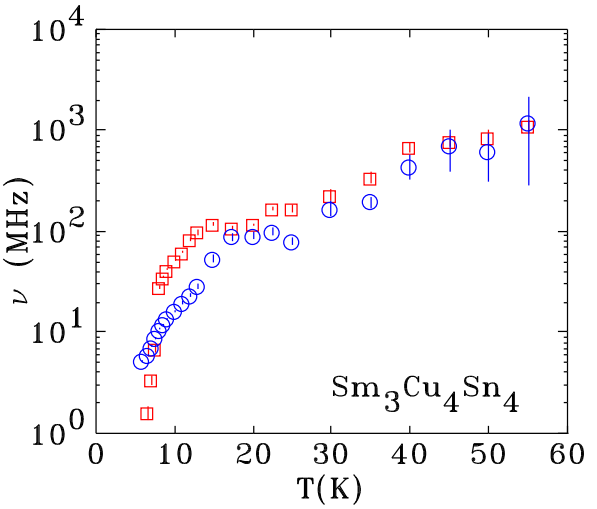

Fig. 18. Temperature dependence of the fluctuation rates for the dynamic fits to the ^{119}Sn Mössbauer spectra of $Sm_3Cu_4Sn_4$. Above 40 K the fluctuation rates are so high that the spectra exhibit motional narrowing and can be fitted equally well using a static paramagnetic doublet, while below 6 K, the fluctuations are too slow to be resolved, and the spectra present as statically ordered.

The observation of an effectively static ordered state in the ^{119}Sn Mössbauer spectra without any sign of order in the neutron diffraction pattern is a result of the very different ways in which the two techniques detect magnetism. Mössbauer spectroscopy is a *local* probe, providing information on the immediate surroundings of the probe nucleus during the fraction of a microsecond over which the γ-nuclear interactions occur. As long as the magnetic environment does not change during

that time, the experiment yields a "static" pattern. By contrast, neutron scattering is a global probe, providing an instantaneous snapshot of the Fourier transform of the spatial arrangements of the nuclei and atomic moments. A fully static, but randomly frozen array of moments yields no coherent scattering and hence no magnetic Bragg peaks are observed. For neutron diffraction to yield a peak, the moments must be *both* static and organized. The results of our measurements on $Sm_3Cu_4Sn_4$ suggest that this system does not exhibit long-range magnetic order, at least not above 3 K.

6.3. $Gd_3Ag_4Sn_4$

Gadolinium-based compounds present extreme challenges to neutron diffraction measurements, and they are usually avoided. As we will now show, this is unfortunate as the results that can be obtained are extremely valuable.

Susceptibility measurements placed the ordering of $Gd_3Ag_4Sn_4$ at 8.2 K, with an easily suppressed feature in the χ_{ac} curve at 22 K that might reflect additional order.[8] Our own susceptibility work confirmed the 8 K feature and identified a second, extremely weak feature in χ''(T) near 30 K.[10] These ambiguous data on transition temperatures clearly demands direct investigation.

The ^{119}Sn Mössbauer spectrum of $Gd_3Ag_4Sn_4$ at 2.3 K consists of two somewhat broadened equal-area sextets (Fig. 19). The temperature dependence of the two hyperfine fields reveals an event at 8 K and the onset of magnetic order at 28.8(2) K. The changes at 8 K clearly reflect only a reorganisation of the magnetic order, and it it puzzling that this, rather than the onset of order at 29 K, should provide the dominant feature in susceptibility measurements. Examination of the quadrupole shift at the two sites provides further insight into the nature of the changes at 8 K.

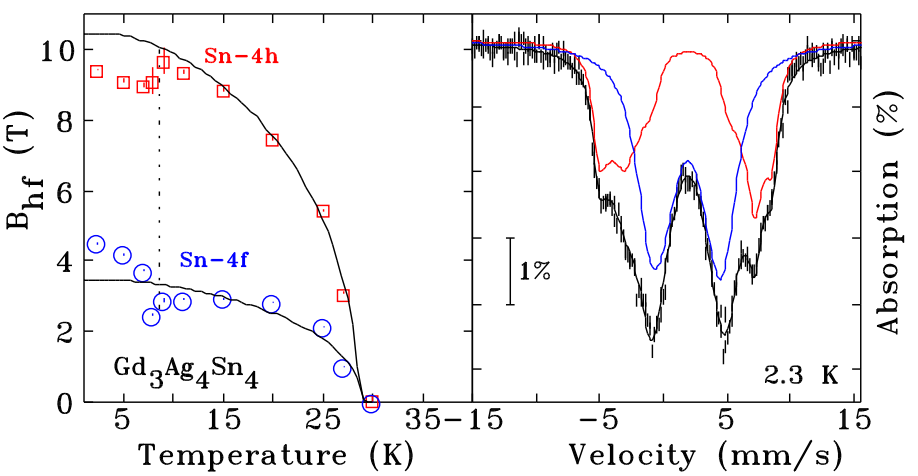

Fig. 19. Left: Temperature dependence of the hyperfine fields (B_{hf}) at the two tin sites in $Gd_3Ag_4Sn_4$ showing the onset of order at 28.8(2) K and a clear break in behavior at 8 K. Right: ^{119}Sn Mössbauer spectrum of $Gd_3Ag_4Sn_4$ at 2.3 K. The two equal-area components used to fit the pattern are also shown.

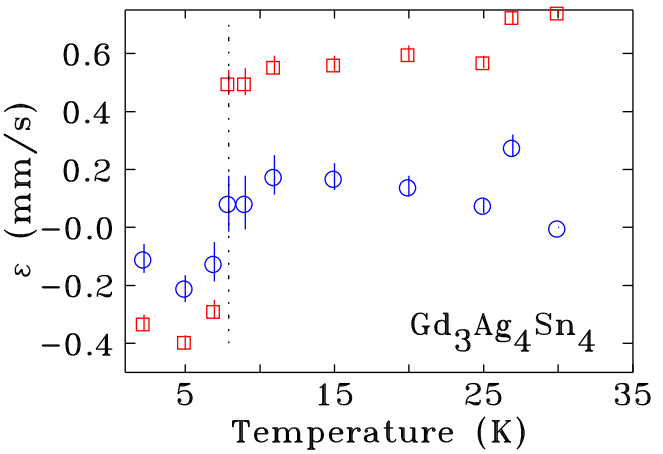

Fig. 20. Temperature dependence of the quadrupole shifts at the two tin sites in $Gd_3Ag_4Sn_4$ showing the reorientation at 8 K. Symbols used correspond to those in Fig. 19.

If we treat the electric field gradient (efg) as axially symmetric, then we can write the observed quadrupole shift ϵ as:

$$\epsilon = \frac{eQV_{zz}}{4}(3\cos{}^2\theta - 1) \tag{1}$$

where θ is the angle between the z-axis of the *efg* (determined by the crystallographic environment) and B_{hf} (due to the surrounding magnetic moments). Within this approximation, ϵ represents the projection of the efg onto B_{hf} at each of the two tin sites. Plotting the temperature dependence of this projection in Fig. 20 reveals evidence for a change in field direction below 8 K in addition to the changes in B_{hf} apparent in Fig. 19. The change in ϵ is close to a factor of -2 at both tin sites. This is best seen at the high-field site where line overlap is less severe and the fits are more reliable: ϵ changes from $\sim$0.6 mm/s above 8 K to ~-0.3 mm/s below 8 K. This change suggests that there is a $\sim 90°$ change in the orientation of the hyperfine field at the two tin sites.

Confirmation of these changes can only come from neutron diffraction. The factor of $\sim$8 larger absorption cross section for gadolinium compared with samarium means that we must reduce the sample size by this factor to compensate. However, the expected Gd moments of 7 μ_B are about fifteen times *larger* than the Sm moments we were able to detect in $Sm_3Ag_4Sn_4$, and the magnetic scattering intensity scales as the *square* of the moment, leading us to expect that the magnetic scattering from $Gd_3Ag_4Sn_4$ should be significantly easier to detect than it was in $Sm_3Ag_4Sn_4$.

Working with 230 mg of $Gd_3Ag_4Sn_4$ loaded into our flat-plate sample mount[30] we were able to obtain the diffraction patterns shown in Fig. 21. Many clear magnetic reflections are evident at 2.8 K demonstrating that this approach does make it possible to obtain neutron diffraction data from Gd-based compounds. Tracking

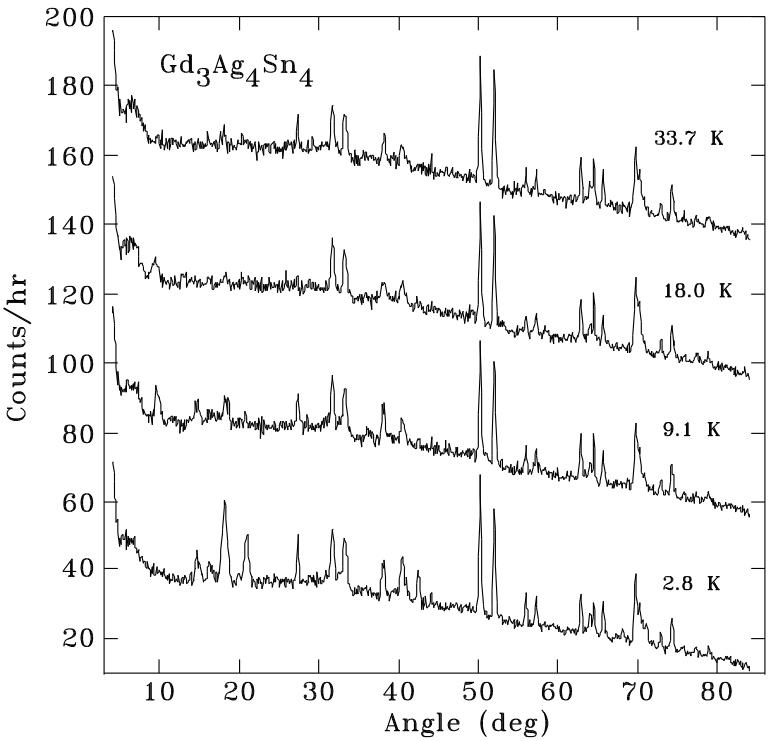

Fig. 21. Neutron diffraction pattern for $Gd_3Ag_4Sn_4$ taken in the paramagnetic state (33.7 K) showing only nuclear peaks, and on cooling to 2.8 K where many magnetic peaks are evident. Measurements were made at a wavelength of 2.3721 Å.

the intensities of some of the stronger reflections (Fig. 22) shows that the onset of long-range magnetic ordering occurs near 25 K, consistent with the earlier ^{119}Sn Mössbauer data, and that a major rearrangement follows near 10 K.

A complete Rietveld analysis using FULLPROF[18] has been carried out,[11] and shows that at 2.8 K (Fig. 23), both the Gd-2d and Gd-4e sublattices adopt antiferromagnetic structures with the moments oriented parallel to the *c*-axis. The Gd-2d structure is incommensurate, while that of the Gd-4e moments is commensurate with the crystal lattice. Above 9 K, the Gd-4e moments reorient onto the *ab* plane and adopt a magnetic structure that is doubled along the *b*-axis and has the moments tilted by $\sim 20^\circ$ from the *a*-axis. The Gd-2d sublattice remains incommensurate but the weak signal and limited number of distinct reflections precludes a more detailed analysis. However, given the strength of the exchange interactions implied by the 29 K ordering temperature, it is very likely that the Gd-2d moments follow the Gd-4e reorientation into the *ab* plane.

Analysis of the tin environments implied by the fitted magnetic structures (presented in Fig. 24) provides confirmation of the derived structures. Both the Sn-4h and the Sn-4f sites each have four Gd-4e neighbors, and at 3 K these are arranged

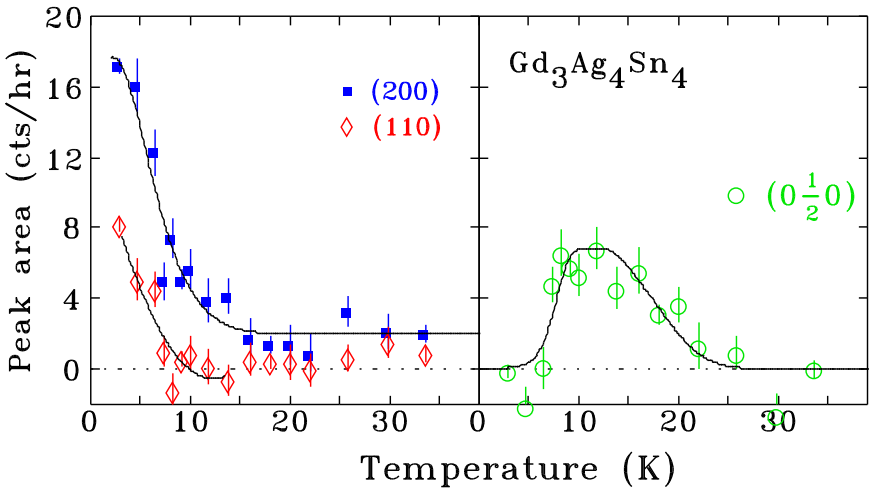

Fig. 22. Temperature dependence of several magnetic reflections from $Gd_3Ag_4Sn_4$. Left: The (200) at 18.1° and (110) at 14.7°, in Fig. 21, appear below 10 K. Right: The $(0\frac{1}{2}0)$ at 9.3° appears near 25 K and is lost on further cooling.

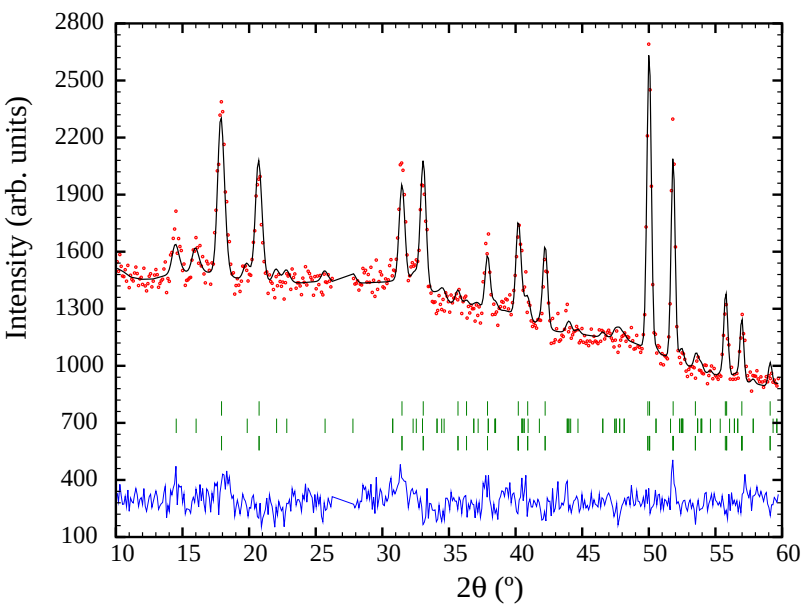

Fig. 23. 2.8 K neutron diffraction pattern for $Gd_3Ag_4Sn_4$ with complete magnetic refinement.[11] The data and calculated pattern are shown at the top, while the lowest trace gives the residuals. The Bragg markers are: nuclear (top), Gd-2d magnetism (middle) and Gd-4e magnetism (bottom). The measurement was made at a wavelength of 2.3721 Å.

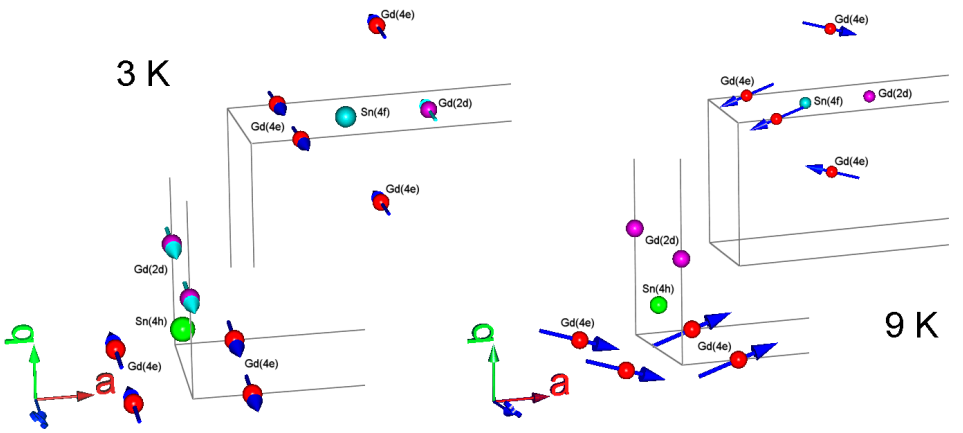

Fig. 24. Magnetic environments of the two tin sites in $Gd_3Ag_4Sn_4$ at 3 K (left) and 9 K (right) derived from our fits of the neutron diffraction patterns. Note: No moments are shown for the Gd-2d sites at 9 K as a complete description of their order above the reorientation temperature could not be detemined (see text).

as two antiparallel pairs, so their net influence at the two tin sites should cancel. The two Gd-2d moments near the Sn-4h site are parallel while the Sn-4f site has a single Gd-2d neighbor leading us to expect the 2:1 hyperfine field ratio noted in several examples above. This prediction compares extremely well with the observed ratio of 2.08:1 at 2.3 K. Above the spin reorientation (shown as 9 K in Fig. 24) we see that the Gd-4e contributions now add at the Sn-4h site and partially cancel at the Sn-4f site, leading to net Gd-4e contributions at both tin sites. If we consider only the effects of the Gd-4e moments, then we find that the transferred fields at the tin sites rotate by 90° (from along the *c*-axis at 3 K to along the *a*-axis at 9 K) consistent with the factor of −2 change in the quadrupole shift (ϵ) in Fig. 20, but the predicted field ratio remains at 2:1 and does not correspond well with the 3.4:1 ratio that is observed. The change in field ratio means that the Gd-2d continue to contribute to the net transferred hyperfine fields above the reorientation temperature. However, in order for the Gd-2d moments to have a significant impact on the total transferred hyperfine fields at the two tin sites, they must be at least close to parallel to the Gd-4e moment directions: i.e. they must also undergo a $\sim 90°$ reorientation along with the Gd-4e moments. The strength of the Gd–Gd exchange interactions implied by the 28.2(2) K ordering temperature coupled with the weak anisotropy typical of Gd^{3+} moments makes it reasonable to expect that the two sublattices rotate together. Without a complete description of the Gd-2d ordering it is not possible to predict the expected hyperfine field ratio in any detail, and many Gd-2d configurations could be consistent with the observed increase in the transferred hyperfine field ratio, however the change in hyperfine field direction and the increase in field ratio both suggest that the Gd-2d moments follow the *c*-axis to *ab* plane rotation of the Gd-4e moments on heating through 9 K. Thus the

combination of neutron diffraction and ^{119}Sn Mössbauer spectroscopy leads naturally to a self consistent and quite detailed description of the magnetic order in $Gd_3Ag_4Sn_4$, both above and below the 9 K spin reorientation.

7. Conclusions

The combination of ^{119}Sn Mössbauer spectroscopy and neutron diffraction is essential to obtaining a complete description of magnetic ordering in the $R_3T_4Sn_4$ compound series. We have shown that the differing sensitivities of the two techniques can be used to great advantage and when used together, the cross-consistency leads to increased confidence in the conclusions.

Much work remains to be done in understanding the physical mechanisms that lead to the complex orderings and re-orderings that occur in these materials. Even the simple question of why *changes* of order so often lead to much clearer susceptibility signatures than the actual onset of order is, as yet, unanswered. However it is clear that Mössbauer spectroscopy and neutron diffraction will continue to play key roles in understanding these, and many other, problems in magnetism.

Acknowledgments

This work was supported by grants from the Natural Sciences and Engineering Research Council of Canada and Fonds québécois de la recherche sur la nature et les technologies. JMC is supported by the Canada Research Chairs program.

References

1. W. Rieger, *Monat. für Chemie* **101** (1970) 449.
2. E. Wawrzyńska, J. Hernández-Velasco, B. Penc, W. Sikora, A. Szytuła and A. Zygmunt, *J. Phys.: Condens. Matt.* **15** (2003) 5279.
3. E. Wawrzyńska, J. Hernández-Velasco, B. Penc, A. Szytuła and A. Zygmunt, *J. Magn. Magn. Mater.* **264** (2003) 192.
4. O. Zaharko, L. Keller and C. Ritter, *J. Magn. Magn. Mater.* **253** (2002) 130.
5. E. Wawrzyńska, J. Hernández-Velasco, B. Penc, A. Szytuła and K. Tomala, *J. Phys.: Condens. Matt.* **16** (2004) 7535.
6. L. K. Perry, J. M. Cadogan, D. H. Ryan, F. Canepa, M. Napoletano, D. Mazzone and P. Riani, *J. Phys.: Condens. Matt.* **18** (2006) 5783.
7. D. H. Ryan, J. M. Cadogan, R. Gagnon and I. P. Swainson, *J. Phys.: Condens. Matt.* **16** (2004) 3183.
8. D. Mazzone, P. Riani, M. Napoletano and F. Canepa, *J. Alloys Comp.* **387** (2005) 15.
9. C. J. Voyer, D. H. Ryan, J. M. Cadogan, L. M. D. Cranswick, M. Napoletano, P. Riani and F. Canepa, *J. Phys.: Condens. Matt.* **19** (2007) 436205.
10. C. J. Voyer, D. H. Ryan, M. Napoletano and P. Riani, *J. Phys.: Condens. Matt.* **19** (2007) 156209.
11. J. M. Cadogan, D. H. Ryan, M. Napoletano, P. Riani and L. M. D. Cranswick, *J. Phys.: Condens. Matt.* **21** (2009) 124201.
12. S. Singh, S. K. Dhar, P. Manfrinetti and A. Palenzona, *J. Alloys Comp.* **298** (2000) 68.

13. S. Singh, S. K. Dhar, P. Manfrinetti and A. Palenzona, *J. Magn. Magn. Mater.* **250** (2002) 190.
14. C. J. Voyer and D. H. Ryan, *Hyp. Int.* **170** (2006) 91.
15. M. Potter, H. Fritzsche, D. H. Ryan and L. M. D. Cranswick, *J. Appl. Cryst.* **40** (2007) 489.
16. A. C. Larson and R. B. von Dreele, "General Structure Analysis System (GSAS)", Los Alamos National Laboratory, Report No. LAUR 86-748 (2004); http://www.ccp14.ac.uk/solution/gsas/.
17. B. H. Toby, *J. Appl. Cryst.* **34** (2001) 210.
18. J. Rodríguez-Carvajal, *Physica B* **192** (1993) 55.
19. T. Roisnel and J. Rodríguez-Carvajal, *Mater. Sci. Forum* **378–381** (2001) 118.
20. E. Wawrzyńska, J. Hernández-Velasco, B. Penc and A. Szytuła, *J. Phys.: Condens. Matt.* **16** (2004) 45.
21. P. Boulet, D. Mazzone, H. Noël, P. Riani, P. Rogl and R. Ferro, *Intermetallics* **7** (1999) 931.
22. L. K. Perry, D. H. Ryan, F. Canepa, M. Napoletano, D. Mazzone, P. Riani and J. M. Cadogan, *J. Appl. Phys.* **99** (2006) 08J502(3).
23. C. J. Voyer, D. H. Ryan and J. M. Cadogan, *J. Appl. Phys.* **105** (2009) 07D508(3).
24. G. Le Caër, B. Malaman, G. Venturini and I. B. Kim, *Phys. Rev. B* **26** (1982) 5085.
25. L. K. Perry, D. H. Ryan and G. Venturini, *Phys. Rev. B* **75** (2007) 144417(7).
26. C. J. Voyer, D. H. Ryan and J. M. Cadogan (unpublished).
27. Ł. Gondek, A. Szytuła, D. Kaczorowski, A. Szewczyk, M. Gutowska and O. Prokhnenko, *Intermetallics* **15** (2007) 583.
28. D. H. Ryan, J. M. Cadogan, C. J. Voyer and I. P. Swainson (unpublished).
29. V. F. Sears, *Neutron News* **3** (1992) 26.
30. D. H. Ryan and L. M. D. Cranswick, *J. Appl. Cryst.* **41** (2008) 198.
31. M. Blume and J. A. Tjon, *Phys. Rev.* **165** (1968) 446.